DOI: 10.1002/((please add manuscript number))
Article type: Communication

Pick and Place Distributed Feedback Lasers using Organic Single Crystals

Suqian Ma, Mengjie Wei, Sai Kiran Rajendran, Markus Karl, Bin Xu, Malte C. Gather, Wenjing Tian, Graham A. Turnbull*, and Ifor D. W. Samuel**

Dr. S. Ma, M. Wei, Dr. S. K. Rajendran, Dr. M. Karl, Prof. M. C. Gather, Prof. G. A. Turnbull, Prof. I. D. W. Samuel
Organic Semiconductor Centre, School of Physics and Astronomy, University of St Andrews, St Andrews KY16 9SS, UK
E-mail: gat@st-andrews.ac.uk; idws@st-andrews.ac.uk
Dr. S. Ma, Prof. B. Xu, Prof. W. Tian
State Key Laboratory of Supramolecular Structure and Materials, Jilin University, Changchun 130012, China
E-mail: wjtian@jlu.edu.cn
Dr. S. Ma
The Key Laboratory of Bionic Engineering, Ministry of Education, Jilin University, Changchun 130025, China

Keywords: solid-state laser, organic semiconductor optoelectronics, optically pumped laser

Abstract: Organic single crystals are of interest for optoelectronic applications due to their highly ordered molecular stacking and small defect concentration, giving the possibility of high mobility and luminescence efficiency. To achieve lasing in large flat single crystals, a simple "pick and place" method of mounting organic single crystals onto distributed feedback gratings is demonstrated. Efficient lasing was achieved with three kinds of active organic single crystals, indicating the potential for broad application of our method for making single crystal lasers using distributed feedback gratings. Detailed investigations of the anisotropic refractive index and waveguide simulations further confirm that distributed feedback can provide efficient ways of fabricating organic single crystal lasers.

Organic π-conjugated materials offer a number of attractive properties for application as miniature, visible solid-state lasers, including their versatility for color-tuning, low-cost, and easy fabrication.[1-3] Organic π-conjugated polymers and dye molecules doped in matrices have been the most widely studied gain materials for organic semiconductor lasers (OSLs).[4-6] Organic single crystals offer advantages over amorphous films of highly ordered molecular stacking and low defect concentration, which give these materials high charge mobilities, efficient photoluminescence and good thermal stability.[7-9] Consequently, they are now emerging as favorable materials for a range of optoelectronic devices, such as OSLs, organic field-effect transistors, and single crystal organic light-emitting diodes.[10-15] In particular, their distinctive combination of optical and electrical properties mean that organic single crystals are well placed to address key issues in realizing electrically pumped OSLs, including the need for high density current injection and low optical losses from contacts.[16,17]

To realize lasing in organic single crystals, there is a need for suitable optical resonators. Currently, most studies related to single crystal lasers are based on micro- or nanocrystals whose flat end facets can act as resonant cavity mirrors for laser feedback.[18-20] For example, Zhao *et al.* have demonstrated that a 2,5-bis(4-biphenylyl)bithiophene (BP2T) hexagonal microdisk constitutes a whispering-gallery-mode resonator, which can provide sufficient feedback for laser oscillation.[21] Song *et al*. have demonstrated high quality perovskite microcrystal lasers on silicon or gold gratings by positioning the microcrystals on the gratings using a tapered fiber equipped with a 3D translation platform.[22-25] Distributed feedback (DFB) gratings would be very attractive alternative structures for optical feedback as they enable a compact resonator to be made with low threshold power density and precise wavelength selection.[26,27] However, their implementation has proved problematic as it has not so far proved possible to grow a single crystal directly on a grating. For sub-millimeter scale two-dimensional (2D) single crystal sheets, several attempts have been made to achieve DFB laser resonators by fabricating periodic grating structures in a photoresist layer above the crystal

surface.[28,29] Sun and co-authors have fabricated gratings directly into the crystal by ablating the crystal surface using laser interference ablation, but damage to the crystals can arise if the laser fluence is not controlled precisely during the procedure.[30,31]

In this paper we demonstrate a simple and efficient "pick and place" method to combine wavelength scale DFB gratings with high-quality sheet-like organic single crystals. By assembling flexible single crystal sheets on top of polymer gratings produced with ultraviolet nanoimprint lithography (UV-NIL),[32,33] we fabricate single frequency lasers with emission wavelength controlled by the feedback gratings. The method was successfully applied to make lasers from different sheet-like single crystal materials, and we relate the laser properties to the optical constants of the birefringent crystals.

Highly emissive sheet-like BDPV2T single crystals (chemical structure in **Figure 1**a) were prepared by the physical vapour transport (PVT) method.[34] Typical crystals (Figure 1b-c) had dimensions of just under a millimeter in each horizontal direction, and 400 nm to several micrometers in height. Upon optical excitation, the crystal emits a broad photoluminescence (PL) spectrum centered at 533 nm as shown in **Figure S1**. On increasing the excitation energy, the crystal shows a narrow amplified spontaneous emission (ASE) spectrum at 533 nm, which means BDPV2T crystals are suitable to be used as a laser gain material. Gratings were fabricated on glass substrates in the resist UVCur21 (Microresist Technologies) by ultraviolet nanoimprint lithography (UV-NIL), and the grating period was selected to be 350 nm to give second-order feedback close to the ASE peak wavelength. To attach the crystal to the grating, an individual BDPV2T crystal was picked up by a fine brush and then carefully placed on the grating structure on top of the glass substrate, as shown in Figure 1d. When one end of the crystal touches the grating, it sticks to the grating, and the rest of the crystal is drawn to the substrate by electrostatic attraction. Once the crystal sticks to the substrate, it is hard to sweep the crystal away using the brush. The tilted scanning electron microscopy (SEM) images in Figure 1e and 1f demonstrate that the single crystal thin layer attaches perfectly to the gratings

with air gaps only between the adjacent ridges. After attaching the crystal to the grating, a thick perfluoro(1-butenylvinylether) polymer (CYTOP) layer was spin coated on top of the sample, which provides mechanical strength can act as an encapsulation layer to protect the crystals from degradation. Figures 1b and 1c show bright field and fluorescence images of an example hexagonal BDPV2T crystal on a one-dimensional (1D) linear grating, visible as the 500 μm by 500 μm deep orange square in Figure 1b.

Next, the sample was excited by a Q-switched diode pumped solid state laser at 355 nm with 1 ns pulse duration and 100 Hz repetition rate. The pump spot of diameter 380 μm was aligned and focused on the region of the crystal directly above the grating using a spherical lens, and the pump energy was adjusted with a neutral density filter. All the measurements were conducted under ambient conditions at room temperature. Emission spectra are shown in **Figure 2**a for a range of pump energies (see **Figure S3** for a semi-log plot). At low pump energy, the emission spectrum was broad, attributed to the steady state fluorescence from the BDPV2T crystal. For a pump density above 122 μJ cm^{-2}, a small peak appeared in the spectrum at 559 nm. On further increasing the pump energy, this peak grew to dominate the spectrum with a linewidth of only 0.08 nm (limited by the resolution of the spectrometer), exhibiting an obvious single mode lasing peak. Figure 2b shows the evolution of the laser output as a function of input pump energy. A clear threshold was observed at 122 μJ cm^{-2}, above which the output intensity grew steeply. The threshold density compared with other single crystal lasers is summarized in **Table S2**.[30] The threshold of our single crystal lasers is higher than the lasers based on π-conjugated polymers,[35] and we attribute this to the relatively large crystal thickness used. For example, the thickness of the crystal used in the experiment in Figure 2 was 637 nm, which is thicker than typical polymer film lasers reported in the literature which commonly have gain layers of 100 - 200 nm thickness. The larger thickness of the crystal may lead to higher threshold in several ways. The first is that most of the excitation light is absorbed in the first 100 nm of

the thick crystal so that only a small part of the total crystal thickness can produce gain. Secondly, the overlap between the waveguide modes of the crystal and the grating may be weaker than the case of a thin polymer film. Finally, the larger thickness can lead to multiple waveguide modes and hence generate mode competition between modes.

To see how many transverse modes are supported in the single crystal sample, angle-resolved PL was measured under excitation from a continuous wave (CW) He-Cd laser at 442 nm. To isolate the transverse electric (TE) modes from transverse magnetic (TM) modes (**Figure S4**), a linear polarizer was aligned parallel to the grating grooves and placed between the sample and the detector. As shown in **Figure 3**a, at normal incidence (0°), an intense intersection at 559 nm corresponding to the lasing peak wavelength can be clearly observed. In addition, there is another intersection at 634 nm and an indistinct one at 713 nm. The intersection at 713 nm is hard to see because it is far in the tail of the PL spectrum of BDPV2T. The strongest TE mode at 559 nm is located in the PL region, thus leading to single mode lasing.

In order to simulate the effective indices of each transverse mode, the in-plane refractive index of the crystal must be known. The anisotropy of molecular packing in the single crystal means that we have to consider its birefringent characteristics when measuring the refractive index. A homemade Fourier imaging microscope equipped with a linear polarizer was used to determine the refractive indices of the crystal.[36-38] Figure 3b shows a microscope image of the hexagonal BDPV2T crystal used for this measurement; the thickness of the crystal was 2480 nm as shown in **Figure S5**. The crystal in-plane *b*-axis and *c*-axis, which can be easily distinguished from the crystal symmetry, were carefully aligned with the linear polarizer during the measurement. When the crystal is illuminated at normal incidence by white light from a lamp, the light reflected between the crystal top and bottom surfaces travel different distances depending on the polarisation and form the thin film interference fringes as shown in **Figure S6**a and Figure S6b, which are along the *c*-axis and *b*-axis, respectively. The group indices at specific wavelengths were calculated as shown in **Figure S7** (black squares for *c*-axis and red circles

for *b*-axis). Fitting these data points to Equation S2, parameters A, B, and C were obtained. The resulting phase refractive indices as a function of wavelength described by the Sellmeier dispersion (Equation S1) is shown in Figure 3c. The refractive index along the *c*-axis is much higher than that along the *b*-axis, which results from the compact molecular π-π stacking and intermolecular interactions along the *c*-axis of BDPV2T crystals as shown in **Figure S8**.[34] The anisotropic molecular packing could also induce anisotropy in optical properties. As shown in **Figure S9** and **S10**, the angle-dependence of emission polarization was measured from an individual crystal using a linear polarizer. The emission showed strongest intensity with the polarizer parallel to crystal *c*-axis, indicating the efficient light coupling with molecular dipoles in this direction.

Notably, the refractive index along the *c*-axis is greater than 2 across the wavelength region measured, and above 2.2 at the ASE peak. A high refractive index is desirable since the waveguide mode profile in multilayer structures tends to be confined more in the high refractive index region. Therefore, in the case of TE modes based on the 1D linear grating, where the light oscillates in the plane of the crystal and parallel to the grating grooves, it may be preferable to align the *c*-axis of the BDPV2T crystal to be parallel with the grating grooves to access the maximum refractive index and strongest light-matter coupling in the gain layer. To test this hypothesis, the lasing properties were investigated as a function of the alignment of the grating grooves with the crystallographic c-axis. As shown in **Figure S11**, as the angle between c-axis and grating grooves is decreased, the emission spectra of the single crystal lasers exhibit a red-shift and the threshold is reduced, due to the increasing refractive index and oscillator strength parallel to the grooves of the linear grating. Waveguide simulations were conducted with finite element modelling (FEM; COMSOL Multiphysics software) using the wavelength obtained from the angle-resolved PL spectra in Figure 3a and the refractive index along the *c*-axis in Figure 3c. As shown in Figure 3d, 3e, 3f, the waveguide supports three TE waveguide modes which are mainly confined in the crystal layer, and the effective indices estimated from FEM

(**Table S3**) agree well with the effective indices calculated from the Bragg condition $\lambda=n_{eff}\Lambda$, where Λ is the grating period of 350 nm. These identify that the laser emission originates from feedback of the TE2 mode.

To investigate the repeatability of laser operation across the area of a single crystal laser, different regions on the same sample were pumped selectively, and the corresponding lasing spectra were recorded as shown in **Figure S13**. The lasing wavelength from different regions are very consistent with variations of less than 0.5 nm. Furthermore, the wavelength controllability of the lasers was explored using gratings of different periods. As shown in **Figure S14**, the peak wavelength of the crystal laser is 558 nm for a grating period of 350 nm, and shifts to 530 nm for a shorter (340 nm) period grating. A series of BDPV2T crystals of different thickness (from 468 nm to 2 μm) were measured and found to show laser action. As shown in **Figure S15**, the lasing thresholds increase with increasing crystal thickness. By solving the Helmholtz wave equation for a three-layer waveguide at 533 nm (ASE peak of BDPV2T crystal) using the index of the crystal *c*-axis, the thickness of the gain layer which can support only one transverse mode is found to be between 22 nm and 186 nm. Therefore, BDPV2T crystals of thickness in this range should have the most effective waveguiding and the lowest threshold. Crystals with thickness larger than 186 nm can support more than one waveguide mode, therefore, mode competition may occur which may contribute to a higher lasing threshold.

The organic single crystals used for the experiment were carefully selected for several attributes. Firstly, all the crystals were obtained from the PVT method so that they are of high quality with smooth surfaces. Secondly, the crystals are slightly flexible which is needed to enable good attachment of the crystals to the gratings. Finally, they all exhibit ASE under pulsed optical pumping. To test the generality of the fabrication method, two other sheet-like organic single crystal materials were also demonstrated using the “pick and place” method. DSB-Me (**Figure**

4a) is a widely studied material [39] with an ASE peak at 482 nm as shown in Figure S1. Good-quality 2D single crystals (inset in Figure 4b) prepared by the PVT method were attached to 290 nm period 1D linear gratings using the method described in Figure 1d. Narrow lasing spectra centered at 480 nm were successfully observed for pump energies exceeding a lasing threshold of 107 μJ cm^{-2} as shown in Figure 4a, 4b. A typical n-type thiophene/phenyl oligomer P2T-CF_3 (chemical structure in Figure 4c) which has an electronic mobility up to 0.18 cm^2 V^{-1} s^{-1} in its thin film [40] was also tested. The green emitting 2D single crystals with ASE peak at 551 nm were assembled with 340 nm period 1D linear gratings. As shown in Figure 4c, 4d, when pumped by the 355 nm pulsed laser, the P2T-CF_3 crystal showed a narrow DFB lasing peak at 560 nm with an excitation threshold of 240 μJ cm^{-2}.

In conclusion, we have successfully developed a simple method through "pick and place" to fabricate DFB lasers from submillimeter-scale 2D organic single crystals. Narrow single frequency laser emission with reasonable excitation thresholds from three different gain crystals BDPV2T, DSB-Me, and P2T-CF_3, demonstrated the broad applicability of the method to make organic single crystal DFB lasers. Detailed investigations of the operation of BDPV2T crystal lasers identified that the laser emission occurs from distributed feedback of the TE2 waveguide mode. More importantly, it may be a stepping stone to realizing electrically pumped lasers from organic single crystals which can combine high charge-carrier mobility with high luminescence efficiency.

Experimental Section

Materials: Three organic fluorescent materials were used as the gain media, with the synthetic route shown in Scheme S1 (Supplementary information). The compound BDPV2T was synthesized in two steps with a yield of 70%. 2,2'-Bithiophene (1) was reacted with *n*-butyllithium and dimethyl formamide to give 5,5'-diformyl-2,2'-bithiophene (2), and then 2 was reacted with diphenylmethane (3) to obtain BDPV2T.[34] Compound DSB-Me was

synthesized in two steps with a yield of 90%. 1,4-Bis(chloromethyl)benzene (4) was reacted with triethyl phosphite to give tetraethyl 1,4-phenylenebis(methylene)diphosphonate (5), then 5 was reacted with 4-methylbenzaldehyde (6) and potassium tert-butoxide to obtain DSB-Me. Compound P2T-CF_3 was synthesized according to the reported literature.[40]

Crystal growth: All the materials were purified by vacuum sublimation before crystal growth. High-quality sheet-like crystals were obtained by the physical vapor transport (PVT) method. In the PVT process, the materials were sublimed at a temperature higher than the melting point at 1 atm, and the material vapor was transferred by argon to cool down at crystallization temperatures and assemble to single crystals.

Grating manufacture: UV-NIL was used to fabricate the DFB gratings according to our previously reported works.[32,33] The gratings were made on an EVG 620 photomask aligner with custom NIL tooling. A soft nanostructured stamp was made by curing a soft UV-curable perfluoropolyether film on the glass substrate with a silicon master structure. Soft-stamps with 0.2 mm thickness were attached to the glass using the adhesion layer 3-(trimethoxysilyl)propyl acrylate. The UV-NIL process begins by loading the soft stamp to the EVG 620 machine. A UVCur21 polymer film on a glass substrate, pre-treated with mr-APS1 adhesion layer, was also placed inside the EVG 620 to contact the soft stamp. Under vacuum and a constant pressure of 950 mbar, UV irradiation was applied to cross-link and harden the UVCur21. After separating the stamp from the substrate, a copy of the silicon master strucutre was left on the UVCur21 layer, which can be used for DFB lasers.

Supporting Information
Supporting Information is available from the Wiley Online Library or from the author. The data that support the findings of this study are openly available in St Andrews research portal at http://dx.doi.org/10.17630/1e47af33-8a1a-4c1a-9505-a141b973cdeb.

Acknowledgements
The authors acknowledge financial support from the Engineering and Physical Sciences Research Council (EPSRC, Hybrid Polaritonics Programme Grant EP/M025330/1), Natural Science Foundation of China (21835001, 51573068, 51773080, 21674041), National Postdoctoral Program for Innovative Talents (BX20180126), China Postdoctoral Science Foundation (2018M641769), Program for Changbaishan Scholars of Jilin Province. S. M. and M. W. acknowledge funding from the China Scholarship Council. M. K. acknowledges funding from the EPSRC DTG (EP/L505079/1). I. D. W. S. acknowledges funding from a Royal Society Wolfson research merit award.

Received: ((will be filled in by the editorial staff))
Revised: ((will be filled in by the editorial staff))
Published online: ((will be filled in by the editorial staff))

References

[1] I. D. W. Samuel, G. A. Turnbull, *Chem. Rev.* **2007**, *107*, 1272.

[2] N. Tessler, *Adv. Mater.* **1999**, *11*, 363.

[3] I. D. W. Samuel, E. B. Namdas, G. A. Turnbull, *Nat. Photonics* **2009**, *3*, 546.

[4] A. J. C. Kuehne, M. C. Gather, *Chem. Rev.* **2016**, *116*, 12823.

[5] G. A. Turnbull, P. Andrew, W. L. Barnes, I. D. W. Samuel, *Appl. Phys. Lett.* **2003**, *82*, 313.

[6] G. Heliotis, R. Xia, G. A. Turnbull, P. Andrew, W. L. Barnes, I. D. W. Samuel, D. D. C. Bradley, *Adv. Funct. Mater.* **2004**, *14*, 91.

[7] R. Li, W. Hu, Y. Liu, D. Zhu, *Acc. Chem. Res.* **2010**, *43*, 529.

[8] S. Hotta, T. Yamao, *J. Mater. Chem.* **2011**, *21*, 1295.

[9] J. Gierschner, S. Varghese, S. Y. Park, *Adv. Opt. Mater.* **2016**, *4*, 348.

[10] S. Ma, J. Zhang, J. Qian, J. Chen, B. Xu, W. Tian, *Adv. Opt. Mater.* **2015**, *3*, 763.

[11] J. Mei, Y. Diao, A. L. Appleton, L. Fang, Z. Bao, *J. Am. Chem. Soc.* **2013**, *135*, 6724.

[12] H. Dong, X. Fu, J. Liu, Z. Wang, W. Hu, *Adv. Mater.* **2013**, *25*, 6158.

[13] H. Uoyama, K. Goushi, K. Shizu, H. Nomura, C. Adachi, *Nature* **2012**, *492*, 234.

[14] R. Ding, J. Feng, F.-X. Dong, W. Zhou, Y. Liu, X.-L. Zhang, X.-P. Wang, H.-H. Fang, B. Xu, X.-B. Li, H.-Y. Wang, S. Hotta, H.-B. Sun, *Adv. Funct. Mater.* **2017**, *27*, 1604659.

[15] K.-H. Kim, J.-L. Liao, S. W. Lee, B. Sim, C.-K. Moon, G.-H. Lee, H. J. Kim, Y. Chi, J.-J. Kim, *Adv. Mater.* **2016**, *28*, 2526.

[16] M. A. Baldo, R. J. Holmes, S. R. Forrest, *Phys. Rev. B* **2002**, *66*, 035321.

[17] D. D. C. Bradley, *Faraday Discuss.* **2014**, *174*, 429.

[18] X. Wang, H. Li, Y. Wu, Z. Xu, H. Fu, *J. Am. Chem. Soc.* **2014**, *136*, 16602.

[19] W. Zhang, Y. Yan, J. Gu, J. Yao, Y. S. Zhao, *Angew. Chem. Int. Ed.* **2015**, *54*, 7125.

[20] X. Wang, Z.-Z. Li, S.-F. Li, H. Li, J. Chen, Y. Wu, H. Fu, *Adv. Opt. Mater.* **2017**, *5,* 1700027.

[21] H. Dong, C. Zhang, X. Lin, Z. Zhou, J. Yao, Y. S. Zhao, *Nano Lett.* **2017**, *17*, 91.

[22] C. Huang, W. Sun, Y. Fan, Y. Wang, Y. Gao, N. Zhang, K. Wang, S. Liu, S. Wang, S. Xiao, Q. Song, *ACS Nano* **2018**, *12*, 3865.

[23] K. Wang, Z. Gu, S. Liu, W. Sun, N. Zhang, S. Xiao, Q. Song, *J. Phys. Chem. Lett.* **2016**, *7*, 2549.

[24] K. Wang, W. Sun, S. Wang, S. Liu, N. Zhang, S. Xiao, Q. Song, *Adv. Optical Mater.* **2017**, *5*, 1600744.

[25] S. Sun, C. Zhang, K. Wang, S. Wang, S. Xiao, Q. Song, *ACS Photonics* **2017**, *4*, 649.

[26] J. Clark, G. Lanzani, *Nat. Photonics* **2010**, *4*, 438.

[27] M. Karl, J. M. E. Glackin, M. Schubert, N. M. Kronenberg, G. A. Turnbull, I. D. W. Samuel, M. C. Gather. *Nat. Comm.* **2018***, 9*, 1525.

[28] R. Ding, H.-H. Fang, Y. Wang, S.-Y. Lu, X.-L. Zhang, L. Wang, J. Feng, Q.-D. Chen, H.-B. Sun, *Organic Electronics* **2012**, *13*, 1602.

[29] H.-H. Fang, R. Ding, S.-Y. Lu, X.-L. Zhang, J. Feng, Q.-D. Chena, H.-B. Sun, *J. Mater. Chem.* **2012**, *22*, 24139.

[30] H.-H. Fang, R. Ding, S.-Y. Lu, J. Yang, X.-L. Zhang, R. Yang, J. Feng, Q.-D. Chen, J.-F. Song, H.-B. Sun, *Adv. Funct. Mater.* **2012**, *22*, 33.

[31] H.-H. Fang, R. Ding, S.-Y. Lu, L. Wang, J. Feng, Q.-D. Chen, H.-B. Sun, *Opt. Lett.* **2012**, *37*, 686.

[32] G. Tsiminis, Y. Wang, A. L. Kanibolotsky, A. R. Inigo, P. J. Skabara, I. D. W. Samuel, G. A. Turnbull, *Adv. Mater.* **2013**, *25*, 2826.

[33] G. L. Whitworth, J. R. Harwell, D. N. Miller, G. J. Hedley, W. Zhang, H. J. Snaith, G. A. Turnbulll, I. D. W. Samuel, *Opt. Express* **2016**, *24*, 23677.

[34] S. Ma, K. Zhou, M. Hu, Q. Li, Y. Liu, H. Zhang, J. Jing, H. Dong, B. Xu, W. Hu, W. Tian, *Adv. Funct. Mater.* **2018**, *28*, 1802454.

[35] E. R. Martins, Y. Wang, A. L. Kanibolotsky, P. J. Skabara, G. A. Turnbull, I. D. W. Samuel, *Adv. Optical Mater.* **2013**, *1*, 563.

[36] T. Yamao, Y. Okuda, Y. Makino, S. Hotta, *J. Appl. Phys.* **2011**, *110*, 053113.

[37] T. Yamao, Y. Taniguchi, K. Yamamoto, T. Miki, S. Ota, S. Hotta, M. Goto, R. Azumi, *Jpn. J. Appl. Phys.* **2007**, *46*, 7478.

[38] T. Yamao, N. Sakamoto, S. Hotta, H. Mizuno, H. Yanagi, *Jpn. J. Appl. Phys.* **2012**, *51*, 11PD03.

[39] R. Kabe, H. Nakanotani, T. Sakanoue, M. Yahiro, C. Adachi, *Adv. Mater.* **2009**, *21*, 4034.

[40] S. Ando, J. Nishida, H. Tada, Y. Inoue, S. Tokito, Y. Yamashita, *J. Am. Chem. Soc.* **2005**, *127*, 5336.

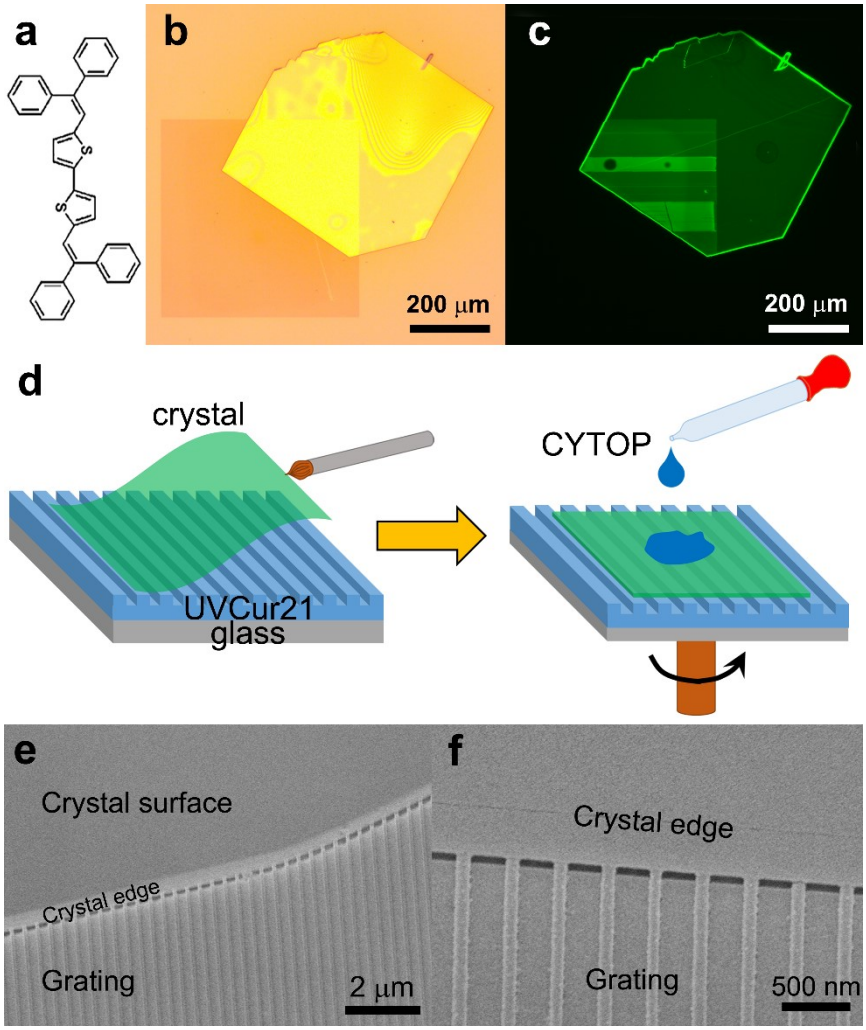

Figure 1. (a) Chemical structure of BDPV2T molecule. (b) Bright field image and (c) fluorescence image of an individual BDPV2T crystal on UV-NIL grating. (d) Schematic diagram of the sample fabrication. (e) 45° tilted and (f) 30° tilted SEM images of an individual BDPV2T crystal on top of 350 nm period linear gratings.

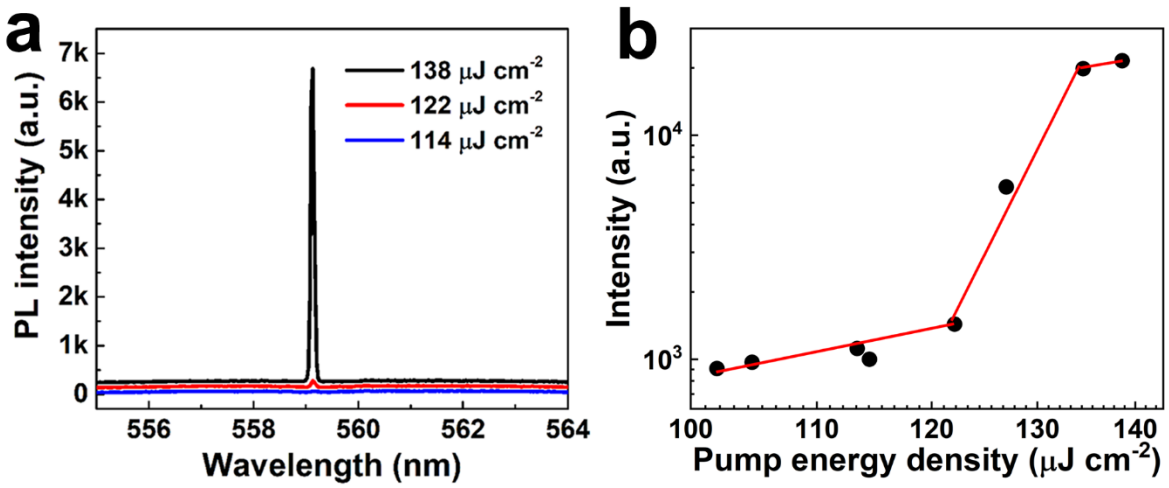

Figure 2. (a) Emission spectra of the single crystal laser on 350 nm grating. The spectra are shown for a pump energy below, at, and well above the lasing threshold. (b) Input-output characteristics of the same sample.

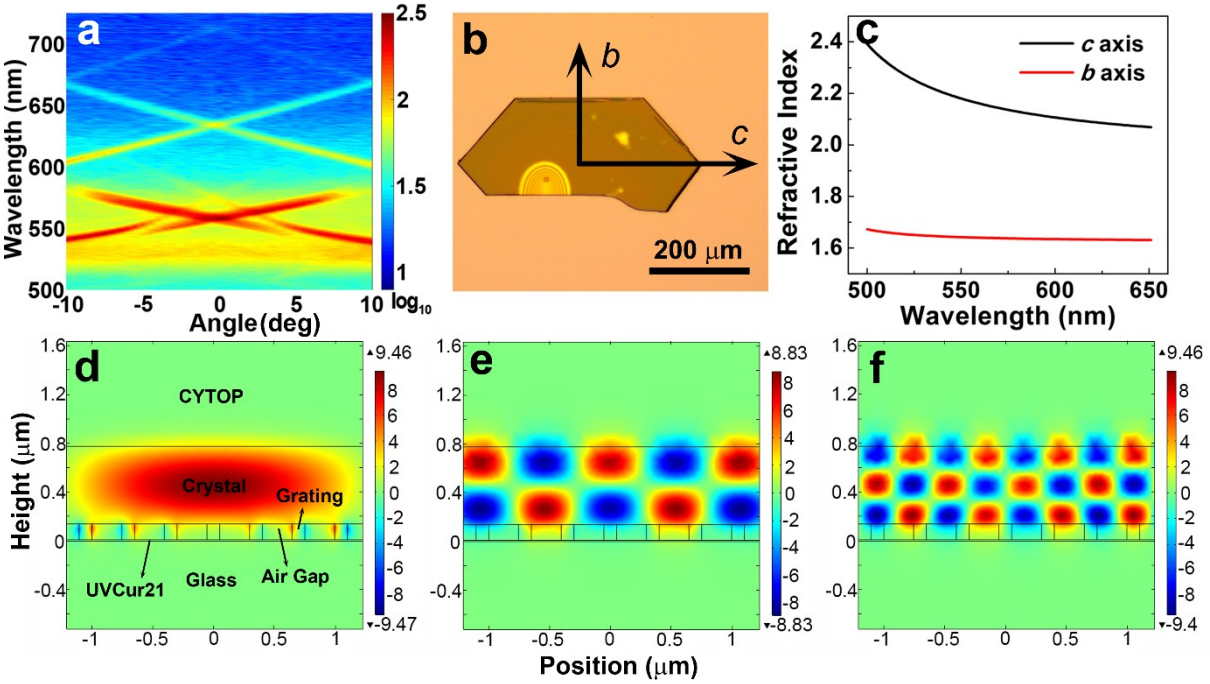

Figure 3. (a) Angle-resolved PL of TE modes. The sample was excited by a 442 nm CW laser, and the excitation energy is below the lasing threshold. (b) Microscope image of crystal used for refractive index measurement. (c) Phase refractive indices of BDPV2T crystal along the *c*-axis and the *b*-axis as a function of wavelength. Waveguide simulation of (d) TE0, (e) TE1, and (f) TE2 modes using FEM. The thickness of the total UVCur21 layer is 140 nm, the depth of the grating is 130 nm (Fig. S12), the grating period is 350 nm with the duty-cycle of 70%, and the thickness of the crystal is 637 nm.

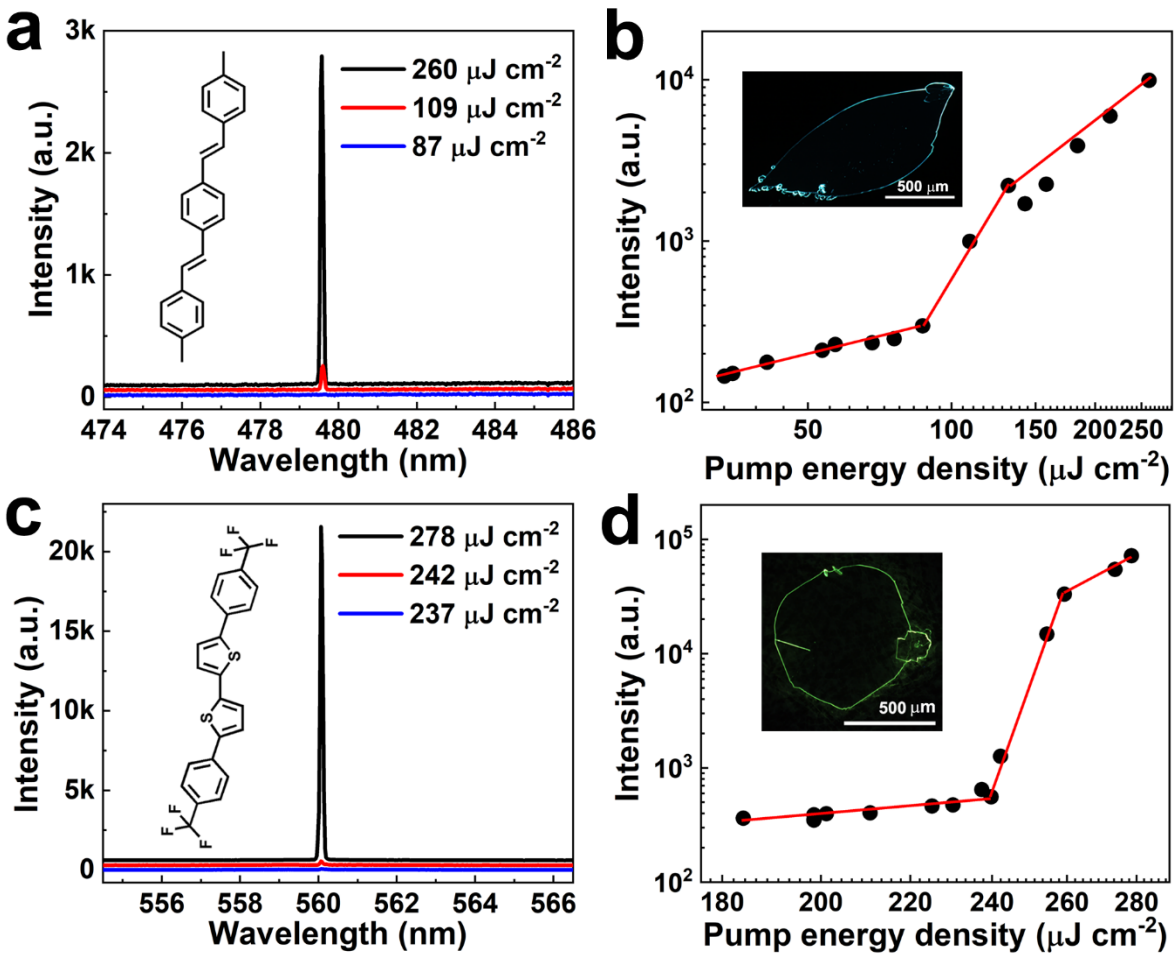

Figure 4. (a) Lasing spectra and (b) input-output characteristics of DSB-Me crystal on the 290 nm 1D linear gratings. (c) Lasing spectra and (d) input-output characteristics of P2T-CF_3 crystal on the 340 nm 1D linear gratings. Insets in b and d show fluorescence microscopy images of the respective sample.

A simple “pick and place” method of mounting organic single crystals onto distributed feedback gratings is demonstrated to achieve lasing in large flat single crystals. Efficient lasing with sharp and narrow peaks are achieved with three kinds of active organic single crystals, indicating the broad applicability of our method for making single crystal lasers using distributed feedback gratings.

Keyword: solid-state laser, organic semiconductor optoelectronics, optically pumped laser

Suqian Ma, Mengjie Wei, Sai Kiran Rajendran, Markus Karl, Bin Xu, Malte C. Gather, Wenjing Tian*, Graham A. Turnbull*, and Ifor D. W. Samuel*

Pick and Place Distributed Feedback Lasers using Organic Single Crystals